Original Article

Structural Health Monitoring
2024, Vol. 23(5) 3253–3275

DOI: 10.1177/14759217231216697
journals.sagepub.com/home/shm

Particle filter-based fatigue damage prognosis by fusing multiple degradation models

Tianzhi Li[1], Jian Chen[2], Shenfang Yuan[2], Dimitrios Zarouchas[3], Claudio Sbarufatti[1] and Francesco Cadini[1]

Abstract

Fatigue damage prognosis always requires a degradation model describing the damage evolution with time; thus, the prognostic performance highly depends on the selection of such a model. The best model should probably be case specific, calling for the fusion of multiple degradation models for a robust prognosis. In this context, this paper proposes a scheme of online fusing multiple models in a particle filter (PF)-based damage prognosis framework. First, each prognostic model has its process equation built through a physics-based or data-driven degradation model and has its measurement equation linking the damage state and the measurement. Second, each model is independently processed through one PF to provide one group of particles. Then, the particles from all models are adopted for remaining useful life prediction. Finally, the particles from each PF are fused with those from all the other PFs to improve their particle diversity, and consequently, to provide better estimation and prognostic performance. The feasibility and robustness of the proposed method are validated by an experimental study, where an aluminum lug structure subject to fatigue crack growth is monitored by a guided wave measurement system.

Keywords

Structural health monitoring, damage prognosis, degradation model, fusion, particle filter, particle diversity, Lamb waves

Introduction

Degradation is an inevitable process that exists in engineering structures. Once a certain level of damage is reached, the proper functionality of the structure can no longer be guaranteed. Necessary inspections should be regularly carried out to avoid such failure, possibly resulting in high financial expenses and long system downtime. To simultaneously guarantee structural safety/reliable operation and reduce maintenance costs, the maintenance is desired to be scheduled just before the damage state reaches a critical level, calling for an advanced damage prognosis technique to provide the structure with remaining useful life (RUL).

Current damage prognosis studies usually have the damage occurring during the degradation process described as a physics-based damage state, such as matrix crack,[1] delamination,[2] or stiffness reduction[3,4] in composites, crack length[5–8] or shape[9] in metal, or a data-driven health indicator (HI)[10–13] extracted from online measured structural health monitoring (SHM) signals. As the structure degradation follows a specific pattern under a certain service condition, the future damage condition can be predicted by a proper model describing such a pattern. A large variety of both physics-based[1,5,6,9] and data-driven[2,3,7,10–12] degradation models have been proposed for such a task. The former resorts to a physics-based law like Paris' law or its extensions, where the degradation rate, for example, strain energy release rate or stress intensity factor, is either analytically calculated[1] or fitted by a data-driven modeling strategy, such as polynomial fitting,[5,6] support vector regression,[9] or neural networks,[14] through numerically simulated data.

[1]Dipartimento di Meccanica, Politecnico di Milano, Milan, Italy
[2]Research Center of Structural Health Monitoring and Prognosis, State Key Laboratory of Mechanics and Control of Mechanical Structures, Nanjing University of Aeronautics and Astronautics, Nanjing, China
[3]Center of Excellence in Artificial Intelligence for Structures, Prognostics & Health Management, Aerospace Engineering Faculty, Delft University of Technology, Delft, The Netherlands

Corresponding author:
Francesco Cadini, Dipartimento di Meccanica, Politecnico di Milano, via La Masa 34, Milan 20156, Italy.
Email: francesco.cadini@polimi.it

On the other hand, the data-driven models are usually built through sufficient physical damage data[2,3,7] or data-driven HIs[10–13] collected during the actual degradation process. The former[2,3,7] typically considers a physical damage state to be measured for one or more specimens, and then it applies those data for model training, such as the crack growth[7] and stiffness reduction[3] depicted by neural networks, or the delamination shape growth modeled by polynomial fitting function.[2] As to the latter,[10–13] at each time instant or load cycle step, some data-sensitive statistical features like mean value, standard deviation, and root mean square (RMS) value are extracted from some online measurements like acoustic emission or acceleration. Those features can either be directly taken as the HI at that step[11] or further processed through a machine learning algorithm to create a more robust HI,[10,12,13] finally producing a database of the HIs during the whole run-to-failure process for training a HI evolution model.

There is no universally best degradation model, as each type of model has its pros and cons.[15] Due to the uncertainties stemming from various sources, including complex degradation mechanisms and environmental influences,[16,17] different prognostic performances manifest when applying the same model to different specimens of the same structure, or when applying different models to the same specimen. For the former, one possibility of improving the prognostic performance is to set the model parameters as unknown components to be online updated by a state estimation technique, such as particle filter (PF), given its demonstrated performances in nonlinear and non-Gaussian problems.

The latter has received plenty of research in battery RUL prediction, where a common strategy to enhance the prognostic robustness is to properly fuse multiple degradation models. Intuitively, all the degradation models and their unknown parameters can be included into state space for PF estimation, and then RUL calculation.[18] This, however, may suffer from the curse of dimensionality and behave poorly with a larger number of degradation models. Alternatively, by eliminating unnecessary components within each model, multiple degradation models can be simplified into one ensemble model with fewer unknown components.[19] On the other hand, to fully explore the potential of each model, current practices[20–22] often have each model processed through one PF to produce one RUL distribution. Subsequently, the final RUL distribution can be derived by computing the average or weighted average of all the RUL distributions. As each model commonly shares the same component like crack length in the crack propagation model[21] or battery capacity in the battery degradation model,[20] the particle diversity for each PF can be further improved by considering the interaction between each model, consequently resulting in a more accurate estimation and prognostic. This, however, has received little attention.

In this context, this work proposes such a scheme by fusing those degradation models within a PF-based prognostic framework. Each degradation model is adopted to formulate a different state space model and to provide one group of particles. Provided with the same state component such as the damage state among all the models, each group of particles can be fused with all the others to improve the diversity, and, consequently, to allow for more robust estimation and prognostic performance. The proposed method is demonstrated by an experimental study, where an aluminum lug structure subjected to fatigue crack growth (FCG) is monitored by an online measurement system of Lamb waves.

The rest of this paper is organized as follows: The section "Novel damage prognosis framework" introduces the four steps of the prognosis framework. The application setup is given in the section "Application setup," while the results of the proposed method applied to the experimental case study are provided in the section "Application results." Finally, the section "Conclusions" concludes this paper.

Novel damage prognosis framework

Figure 1 presents the four main steps of the proposed damage prognosis framework. First, each prognostic model is formulated in state space using either a physics-based or data-driven degradation model. Second, each model is independently processed through one PF to provide one group of particles. Then, all the samples of damage state and RUL are used for damage quantification and RUL prediction, respectively. Finally, given the same state component such as the damage state among different models, each group of particles can be fused with all the others to improve the diversity. Compared to the traditional method,[5,6] where only one prognostic model is processed through PF for RUL prediction, the main novelty of the proposed method is that a fusion scheme is online implemented to fuse the particles from different prognostic models for improving the particle diversity, and consequently, the overall estimation and prognostic accuracy.

Prognostic model

The degradation behavior of a structure can be in general described as:

$$x_k = f_l(x_{k-1}, \boldsymbol{\theta}_l) \tag{1}$$

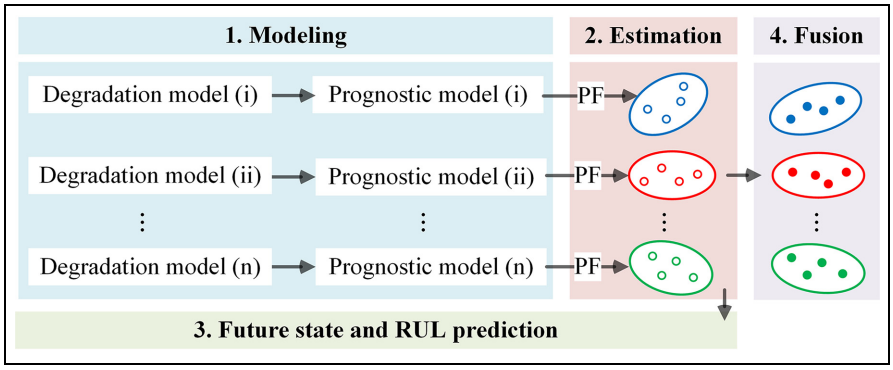

Figure 1. Schematics of the proposed framework.

where x is the damage state like the crack length in metal, $f_l(\cdot)$ is the l-th degradation function, $\boldsymbol{\theta}_l$ is a vector of function coefficients, such as the parameters C and m in Paris' law, and the subscript k denotes the k-th time step. The parameter $\boldsymbol{\theta}_l$ usually varies in different specimens of the same structure due to the uncertainties arising from the degradation process, so they are taken as unknown variables to be estimated. To this aim, following a popular approach, they are added into an augmented state vector:

$$\begin{bmatrix} \boldsymbol{\theta}_{l,k} \\ x_k \end{bmatrix} = \begin{bmatrix} \boldsymbol{\theta}_{l,k-1} + \boldsymbol{\omega}_{\theta,l,k} \\ f_l(x_{k-1}, \boldsymbol{\theta}_{l,k}, \omega_k) \end{bmatrix} \tag{2}$$

where ω and $\boldsymbol{\omega}_{\theta,l}$ are the process noises for the damage state and the parameters, respectively.

Then, a direct or indirect measurement system is usually used for model updating. The former involves a direct measure of the damage state, such as the case of the crack length in a metallic structure observed by a caliper[7,23] or that of matrix cracking density and delamination length in composites measured by X-rays.[1,24,25] In case the damage state cannot be directly measured, one may refer to an indirect measurement system, such as fiber Bragg grating strain sensors[26,27] or Lamb wave-based monitoring systems,[6,28,29] to infer the damage state through a measurement equation describing the relationship between the damage state and the measurement (mostly specific damage-sensitive statistical feature extracted from measured signals). Such an equation is usually built through a data-driven modeling technique, including neural networks,[26,27] polynomial functions,[6] the leave-one-out method,[29] or Gaussian process regression.[28]

With a proper measurement y (which, in most cases, is the statistical feature mentioned above) for inferring the unknown damage state, the measurement equation in a PF-based damage prognosis can be formulated as:

$$y_k = g(x_k) + \nu_k \tag{3}$$

where $g(\cdot)$ is usually a data-driven function describing the relationship between the damage state and the measurement, ν_k is the measurement noise. Given that the measurement Equation (3) is usually built by the data from some specimens, the bias between the measurements from a test specimen and those predicted by this equation is unavoidable. Such an equation fails to be online updated or to take the bias into account, possibly resulting in inaccurate prognostics in case of large-level bias.[6] In this context, the prognostic model[6] with a bias parameter b included for online estimation is used in this study, and it is formulated as:

$$\begin{cases} \boldsymbol{z}_{l,k} = \begin{bmatrix} \boldsymbol{\theta}_{l,k} \\ x_k \\ b_k \end{bmatrix} = \begin{bmatrix} \boldsymbol{\theta}_{l,k-1} + \boldsymbol{\omega}_{\theta,l,k} \\ f_l(x_{k-1}, \boldsymbol{\theta}_{l,k}, \omega_k) \\ b_{k-1} + \omega_{b,k} \end{bmatrix} \\ y_k = g(x_k) + b_k + \nu_k \end{cases} \tag{4}$$

where b is the bias parameter and ω_b is its corresponding process noise, and $\boldsymbol{z}$ is the state vector including the model parameter, damage state, and bias.

Note that each degradation model has its version of Equation (4). More specifically, each model has a different process equation from the others; thus, the number of models built in this framework is equal to the number of available degradation models. On the other hand, to provide an accurate comparison between the performance of multiple degradation models and that of one model, this study has the same measurement equation shared by each prognostic model. Note that the use of the same measurement equation among different prognostic models is not mandatory. Even when each model has a different measurement equation, the damage state is always the component shared by each model and thus can be used to improve the particle diversity.

Particle filter-based estimation

In a Bayesian approach, the k-th-step unknown state vector $\boldsymbol{z}_{l,k}$ can be inferred from the observation as:

$$p(\boldsymbol{z}_{l,k}|\boldsymbol{y}_{1:k-1}) = \int p(\boldsymbol{z}_{l,k}|\boldsymbol{z}_{l,k-1})p(\boldsymbol{z}_{l,k-1}|\boldsymbol{y}_{1:k-1})\mathrm{d}\boldsymbol{z}_{l,k-1} \quad (5)$$

$$p(\boldsymbol{z}_{l,k}|\boldsymbol{y}_{1:k}) \propto p(y_k|\boldsymbol{z}_{l,k})p(\boldsymbol{z}_{l,k}|\boldsymbol{y}_{1:k-1}) \quad (6)$$

where $\boldsymbol{y}_{1:k}$ is the measurement vector collected from time step 1 to k, the symbol $\propto$ means "proportional to," the transition distribution $p(\boldsymbol{z}_{l,k}|\boldsymbol{z}_{l,k-1})$ and the likelihood function $p(y_k|\boldsymbol{z}_{l,k})$ are the process and measurement equations, respectively, $p(\boldsymbol{z}_{l,k}|\boldsymbol{y}_{1:k-1})$ and $p(\boldsymbol{z}_{l,k}|\boldsymbol{y}_{1:k})$ represent the prior and posterior probability distribution function (PDF), respectively.

Given that the analytical solution of Equations (5) and (6) can hardly be acquired in a nonlinear and non-Gaussian system like Equation (4), an efficient state estimation, that is, the sampling importance resampling (SIR) PF,[30] is used in this study. Table 1 lists the pseudo-code of the SIR PF. Note the number of PFs implemented at each step is equal to the number of models.

RUL prediction

By resorting to the degradation model Equation (1) and the posterior PDF of the damage state and its growth parameters, the prognostic step enables the prediction of future damage state at any step ahead of the k-th one. Once the predicted state reaches a pre-defined threshold of the damage state l_{th}, above which the structure fails, the RUL is taken as the multiplication of the number of prediction steps and the number of load cycles ΔN in one step. The pseudo-code of the above procedure for the l-th prognostic model is summarized in Table 2. Note that the RUL is independently predicted through each degradation model, and then multiple groups of RUL samples are merged to produce the RUL distribution.

Fusion for improving particle diversity

In the SIR PF resampling procedure, the particles with large weights are duplicated and those with small weights are eliminated. As a result, the diversity of the particles tends to decrease over time, which can limit the PF performance. This phenomenon is commonly referred to as particle impoverishment. It has been well elaborated that the strategies for improving particle diversity can lead to more robust state and parameter estimation.[31,32]

The proposed method has multiple prognostic models providing multiple groups of particles, among which they share some state components, that is, the damage state and bias parameter of Equation (4). The two components can be included in a vector as:

$$\boldsymbol{s}_k = \begin{bmatrix} x_k \\ b_k \end{bmatrix} \quad (7)$$

This enables the possibility of improving the sample diversity of those shared components for each PF.

The objective of this paper is to verify the applicability of the proposed method to diverse algorithms aimed at enhancing diversity. To achieve this goal, the paper employs the crossover and mutation operators, two widely used genetic operators for addressing such problems,[31,32] to the shared components mentioned earlier in a separate manner. For each time step and each PF, the crossover operator is implemented as follows:

$$\boldsymbol{s}^i_{k,l} = \alpha \boldsymbol{s}^i_{k,l} + \frac{1-\alpha}{n-1}\underbrace{\left(\boldsymbol{s}^i_{k,1} + \ldots + \boldsymbol{s}^i_{k,l-1} + \boldsymbol{s}^i_{k,l+1} + \ldots + \boldsymbol{s}^i_{k,n}\right)} \quad (8)$$

where the i-th sample $\boldsymbol{s}^i_{k,l}$ contains a vector of the shared components from the l-th PF, while the samples from all the other PFs are included in the horizontal curly bracket, n is the number of PFs (or models) used, and α is a coefficient within a range of [0 1]. On the other hand, when the mutation operator is applied to the l-th PF, a certain percentage of samples of the shared components from that PF is replaced by some samples randomly selected from all the other PFs.

Notice that the proposed method is generic enough so that the other operators can be included. The fusion of multiple degradation models intends to provide multiple groups of well-distributed samples, while the algorithm for adopting all the samples to improve the diversity for each group can be user-defined. Interested

Table 1. Sampling importance resampling particle filter.

Initialization: draw N_p particles $\left\{\mathbf{z}^i_{l,0} : i = 1, 2, \ldots, N_p\right\}$ from the distribution $p(\mathbf{z}_{l,0})$
For k = 1, 2,…,
  Prediction in PF: draw N_p particles $\left\{\mathbf{z}^i_{l,k} : i = 1, 2, \ldots, N_p\right\}$ by $\mathbf{z}^i_{l,k} \sim p\left(\mathbf{z}_{l,k}|\mathbf{z}^i_{l,k-1}\right)$
  Weight update: calculate the particle weight w^i_k through $w^i_k \propto p\left(\mathbf{y}_k|\mathbf{z}^i_{l,k}\right)$, and assign its normalized form $\tilde{w}^i_k$ to each particle $\mathbf{z}^i_{l,k}$
  Resample for those particles based on the normalized weights
End

Table 2. Calculation of future state and RUL at time step k for the l-th model.

Initialization: set $\{x_k^{i,0}: i=1,2,\ldots,N_p\}$ as $\{x_k^i: i=1,2,\ldots,N_p\}$
For i = 1: N_p
  j = 0
  While $x_k^{i,j} < l_{th}$
    Calculate the future state $x_k^{i,j+1}$
    by $x_k^{i,j+1} = fl\left(x_k^{i,j}, \boldsymbol{\theta}_{l,k}^i\right)$
    j = j + 1
  End
  $RUL_{l,k}^i = j \times \Delta N$
End

RUL: remaining useful life.

readers may refer to Refs. 33 and 34 for those algorithms, but not mentioned here for simplicity.

Application setup

This section includes the experimental study,[28] numerical study,[5] signal processing, state-space modeling, and the creation of the target crack length and features. The experimental setup of the fatigue tests and Lamb wave monitoring is briefly introduced in the section "Experimental study." The Lamb wave simulations for modeling the measurement equation are presented in the section "Numerical study." The Lamb waves from the experimental and numerical studies are adopted to provide the statistical feature for damage quantification in the section "Feature extraction." The section "Typical degradation models" presents three typical degradation models used in practices, while the section "State space modeling and PF parameters" shows the state space modeling and the PF parameters. The section "Target crack growth and features" illustrates the creation of the target crack growths and their corresponding features using all the experimental specimens.

Experimental study

Figure 2(a) and (b) shows the fatigue test of an aluminum lug structure and a Lamb wave-based monitoring system,[28] respectively. The structure has a thickness of 5 mm and a through hole with a diameter of 5 mm. The latter has a 2-mm-long notch created on the edge for initiating the crack growth. The MTS810 electro-hydraulic servo material test system is used to provide the sinusoidal tensile fatigue load, with maximum value, minimum value, and frequency set as 18 kN, 0.1, and 10 Hz, respectively.

Figure 2(c) shows an image collected by a digital microscope for observing the crack length. The scale lines are equally spaced by 1 mm. A pre-cracking step is performed at the beginning of the fatigue test until the crack length reaches 3 mm. The fatigue loading is occasionally paused during the test, and then a static tensile load of 18 kN is applied to the specimen for better visualization of the crack. The crack length is considered to increase by 1 mm once the crack tip reaches the next line. At each measured crack length, for example, 3 mm or 4 mm, one transducer serves as the actuator providing a 3-cycle Hanning-windowed sine burst with a central frequency of 160 kHz, and another one is the sensor collecting the Lamb waves with a sampling frequency of 50 MHz.

Figure 3(a) depicts the FCG trajectories of six specimens, namely S1–S6. These specimens exhibit variations that primarily result from uncertainties in the manufacturing process and specimen assembly, among other factors. The initial crack length and the threshold for RUL calculation are 3 mm and 22 mm, respectively. It is noteworthy that the crack growth data of specimen S6 will be utilized to determine the coefficients of degradation models, as discussed in sections "Typical degradation models" and "State space modeling and PF parameters." Conversely, the data from specimens S1 to S5 will serve for testing purposes.

Figure 3(b) illustrates the experimental Lamb waves, with a duration of 1.2×10^{-4} s, at three different crack lengths. The first wave package is crosstalk, which arises from the electromagnetic induction between the actuator and sensor circuits. To account for this, the start of the crosstalk (SoC) is considered the time when the actuator applies the excitation to the structure.[35] The analytical arrivals of the S_0 and A_0 waves are approximately equivalent to the summation of the SoC and the S_0 wave time-of-flight (ToF), and to that of the SoC and the A_0 ToF, respectively. Interested readers can refer to Refs. 5 and 6 for further details on the calculation. Typically, increasing crack lengths result in amplitude reductions of the S_0 waves, which cause variations in the features extracted from these waves.

Numerical study

Figure 4 shows the Lamb wave numerical simulations under different crack lengths, which has been well detailed in Li et al.,[5] thus briefly introduced here. ABAQUS EXPLICIT is used to provide the numerical S_0 Lamb waves of the structure at nine crack lengths {3, 5, 8, 10, 12, 15, 18, 20, 22 mm}. Two symmetric out-of-plane pressures, whose amplitudes are the same as the excitation used in the experiment, are applied within the circles (same as the actuator shape) on the two sides of the plate at each crack length. The out-of-plane displacements at the center of the sensor location are taken as the numerical Lamb wave.

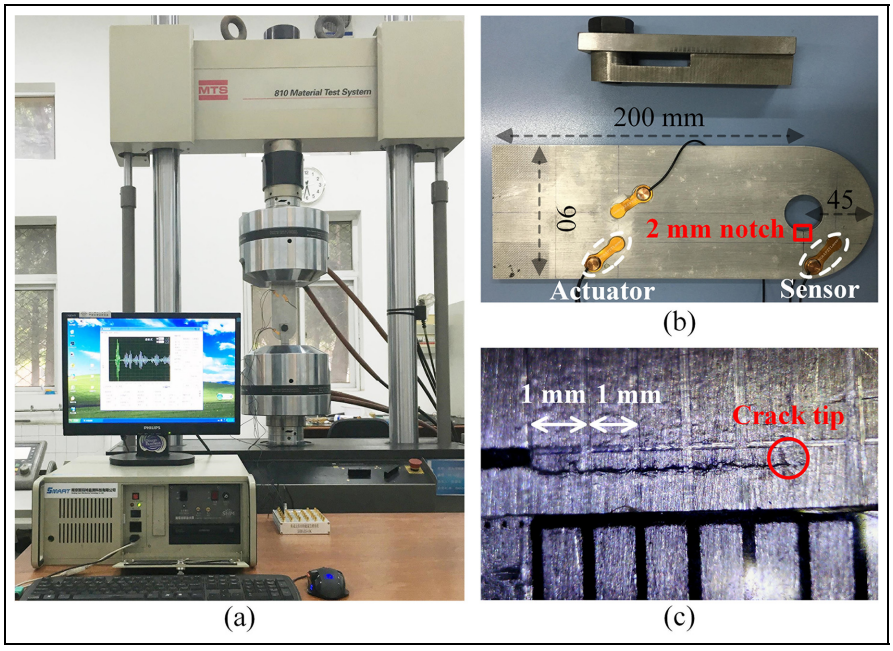

Figure 2. Experimental setup: (a) fatigue test, (b) Lamb wave measurement system, and (c) crack and scale lines.

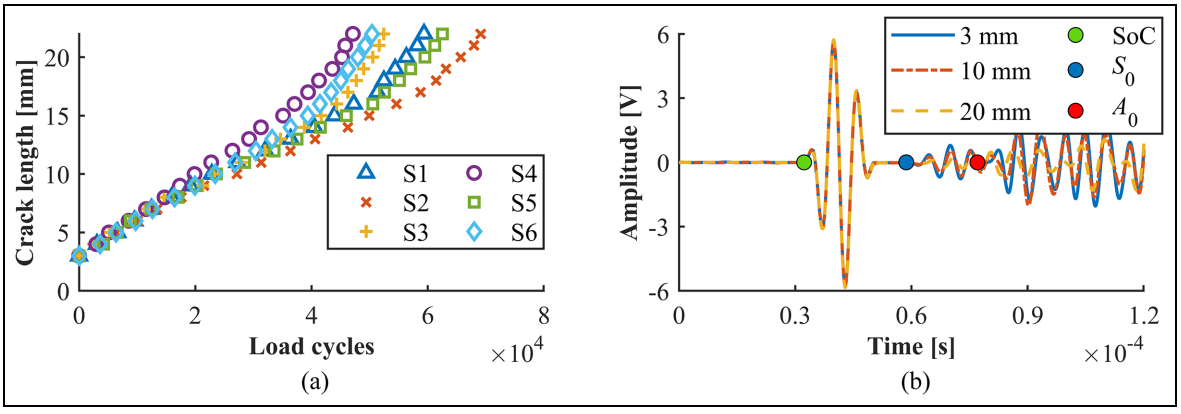

Figure 3. Fatigue crack growths with Lamb wave monitoring: (a) crack growths of specimens S1–S6 and (b) Lamb wave signals at three crack lengths from S1.
SoC: start of crosstalk.

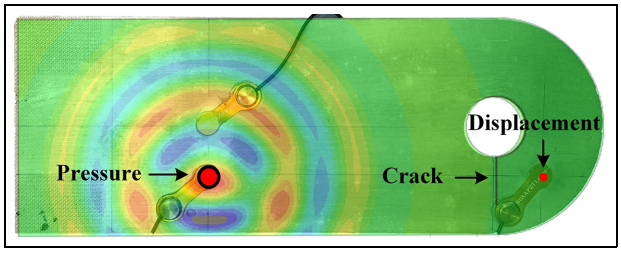

Figure 4. Numerical setup.

Figure 5(a) and (b) shows the comparisons of the numerical and experimental (specimen S1) Lamb waves at crack lengths of 3 mm and 20 mm, respectively. The crosstalk of the experimental signal is replaced by zero values for simplicity. The numerical S_0 Lamb waves satisfactorily agree with the experimental ones before 4×10^{-5} s, and thus can be adopted for modeling the measurement equation relating the crack length and some sort of Lamb wave-based statistical feature.

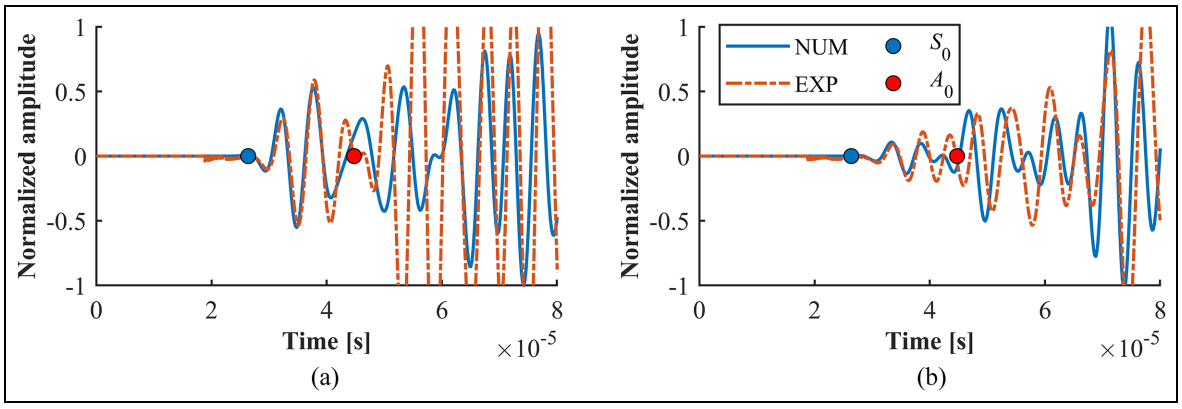

Figure 5. Numerical and experimental (specimen S1) Lamb waves at two crack lengths: (a) 3 mm crack and (b) 20 mm crack.

Table 3. Three typical degradation models used in practice.

Model	Literature	Which type of model	General expression	The model used in this study
1	5 and 6	Physics based	$x_k = x_{k-1} + \Delta N_k f_1(x_{k-1})$	$x_k = x_{k-1} + C(\Delta K(x_{k-1}))^m \Delta N_k$
2	3	Data driven	$x_k = x_{k-1} + \Delta N_k f_2(x_{k-1})$	$x_k = x_{k-1} + \Delta N_k \left(p_1 x_{k-1}{}^3 + p_2 x_{k-1}{}^2 + p_3 x_{k-1} + p_4\right)$
3	7	Data driven	$x_k = f_3(N_k)$ or $x_k = f_3(t_k)$	$x_k = q_1 N_{k-1}{}^3 + q_2 N_{k-1}{}^2 + q_3 N_{k-1} + q_4$

(i) The function $f_1(\cdot)$ is derived from physical knowledge, while $f_2(\cdot)$ and $f_3(\cdot)$ from experimental data, (ii) N and t denote the number of load cycles and the time, respectively, and ΔN is the number of load cycles included at one time step and (iii) the parameters C and m and the polynomial coefficients p_1, p_2, p_3, p_4, q_1, q_2, q_3, and q_4 will be fitted from the crack growth data of experimental specimen S6 for initializing the particle filter.

Feature extraction

Similar to the work[5] from the same authors, the feature is extracted from the Lamb wave signals within a properly selected time window, whose start and width are defined as the S_0 arrival and 10^{-5} s, respectively. Given the demonstrated performances of RMS-based features in the prognostic investigation,[36] it is chosen in this study and defined as follows:

$$\mathrm{RMS}_l = 1 - \frac{\mathrm{rms}(f_l)}{\mathrm{rms}(f_r)} \tag{9}$$

Note that f_r and f_l are the windowed Lamb waves at the initial crack length of 3 mm and another crack length l mm, respectively, and the function "rms" is the root mean square value of an individual set of signals.

The above processing is implemented for the numerical Lamb waves and the experimental Lamb waves from each of the specimens S1–S5, as shown in Figure 6. The satisfactory match between the numerical and experimental features enables the feasibility of adopting the numerical data for modeling the measurement equation. The features from experimental specimens S1–S5 will be processed in the section "Target crack growth and features" for testing the proposed method.

Typical degradation models

Table 3 lists three typical degradation models adopted in current prognostic practices. The rate of damage evolution in the first two models is characterized as a function of the current damage state, which can be determined from either theoretical knowledge or empirical data. The last model considers the damage state as a function of time or the number of load cycles, and it can only be built through some experimental data. This study adopts all three types of models, as detailed below.

The first model used in this study adopts Paris's law to describe the crack growth. The two parameters C and m are the empirical values, and the calculation of the stress intensity factor range ΔK is taken from the work of some of the same authors,[6]

$$\Delta K(x) = 1.43\times10^{-3}x^3 + 5.63\times10^{-1}x^2 - 13.5x + 497.8 \tag{10}$$

The two data-driven functions $f_2(\cdot)$ and $f_3(\cdot)$ in the last two models used in this study are built by the third-order polynomial fitting function, due to its demonstrated performance in damage prognosis investigation,[2] although other approaches, for example, machine learning-based, can be used in principle. The parameters C and m and

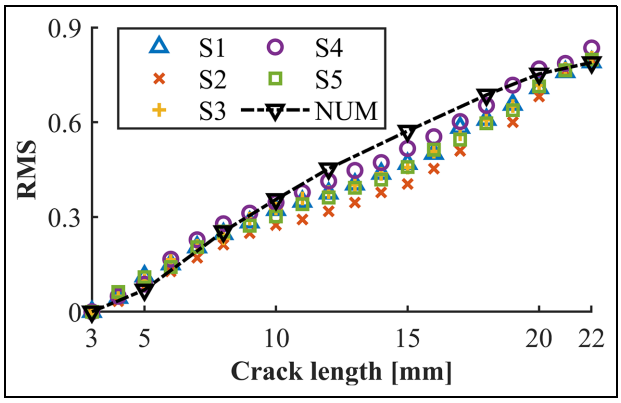

Figure 6. Root mean square (RMS) values at different crack lengths from numerical and experimental studies.

the polynomial coefficients p_1, p_2, p_3, p_4, q_1, q_2, q_3, and q_4 will be acquired through the experimental data of specimen S6 for initializing each PF.

State space modeling and PF parameters

The three degradation models lead to three prognostic models as below:

$$\begin{cases} z_{1,k} = \begin{bmatrix} \ln C_k \\ m_k \\ x_k \\ b_k \end{bmatrix} = \begin{bmatrix} \ln C_{k-1} + \omega_{c,k} \\ m_{k-1} + \omega_{m,k} \\ x_{k-1} + e^{\omega_{1,k}} C_k (\Delta K(x_{k-1}))^{m_k} \Delta N_k \\ b_{k-1} + \omega_{b,k} \end{bmatrix} \\ y_k = g(x_k) + b_k + \nu_k \end{cases} \tag{11}$$

$$\begin{cases} z_{2,k} = \begin{bmatrix} p_{1,k} \\ p_{2,k} \\ p_{3,k} \\ p_{4,k} \\ x_k \\ b_k \end{bmatrix} = \begin{bmatrix} p_{1,k-1} + \omega_{p,1,k} \\ p_{2,k-1} + \omega_{p,2,k} \\ p_{3,k-1} + \omega_{p,3,k} \\ p_{4,k-1} + \omega_{p,4,k} \\ x_{k-1} + e^{\omega_{1,k}} \\ (p_{1,k} x_{k-1}^3 + p_{2,k} x_{k-1}^2 + p_{3,k} x_{k-1} + p_{4,k}) \Delta N_k \\ b_{k-1} + \omega_{b,k} \end{bmatrix} \\ y_k = g(x_k) + b_k + \nu_k \end{cases} \tag{12}$$

$$\begin{cases} z_{3,k} = \begin{bmatrix} q_{1,k} \\ q_{2,k} \\ q_{3,k} \\ q_{4,k} \\ x_k \\ b_k \end{bmatrix} = \begin{bmatrix} q_{1,k-1} + \omega_{q,1,k} \\ q_{2,k-1} + \omega_{q,2,k} \\ q_{3,k-1} + \omega_{q,3,k} \\ q_{4,k-1} + \omega_{q,4,k} \\ p_{1,k} N_k^3 + p_{2,k} N_k^2 + p_{3,k} N_k + p_{4,k} + e^{\omega_{2,k}} \\ b_{k-1} + \omega_{b,k} \end{bmatrix} \\ y_k = g(x_k) + b_k + \nu_k \end{cases} \tag{13}$$

where the state vectors z_1, z_2, and z_3 have four, six, and six components, respectively, $\omega_1 \sim \mathcal{N}\left(-\frac{\sigma^2}{2}, \sigma^2\right)$ is the unbiased Gaussian process noise with the standard deviation σ,[23] $\omega_{p,1}$, $\omega_{p,2}$, $\omega_{p,3}$, $\omega_{p,4}$, $\omega_{q,1}$, $\omega_{q,2}$, $\omega_{q,3}$, $\omega_{q,4}$, ω_2 and ω_b are zero-mean Gaussian process noises, the measurement y is the RMS feature, $g(\cdot)$ is a function describing the relationship between the crack length and RMS feature. Similar to the work from some of the same authors,[5] the function $g(\cdot)$ is a fourth-order polynomial regression fitted by the numerical RMS features at different crack lengths:

$$g(x) = 7.42\times10^{-6}x^4 + 4.20\times10^{-4}x^3 + 7.27\times10^{-3}x^2 + 4.43\times10^{-3}x + 7.37\times10^{-2} \tag{14}$$

Each prognostic model mentioned above is nonlinear and non-Gaussian because of the non-linearities of the degradation model and the function $g(\cdot)$, and the non-Gaussian noise e^{ω}, respectively. Note that these models share two state components, that is, the crack length x, and the bias parameter b. For each PF, the distribution of the samples of the two components will be modified with those from all the other PFs through either the mutation or the crossover operator.

Kernel smoothing[37] is adopted to improve the accuracy of estimating the time-invariant parameters ln C, m, p_1, p_2, p_3, p_4, q_1, q_2, q_3, and q_4. The parameter m is taken as an example for the illustration as follows:

$$m_k = \sqrt{1-h^2}\, m_{k-1} + \left(1 - \sqrt{1-h^2}\right)\hat{m}_{k-1} + \omega_{m,k} \tag{15}$$

where h is the smoothing parameter selected within a range of [0 1], and $\hat{m}$ are the mean of the samples for the parameter m.

Table 4 shows the values of the PF parameters used in this study, most of which are determined from the works of the same authors.[2,5,6] As to the model fusion, the coefficient α for the crossover operator is set to 0.95, while the mutation percentage of the mutation operator to 10%. The criteria for the selection of initial distribution or range, process noise, and standard deviation in likelihood are given below, while more details on sensitivity analyses can be found in Refs. 26, 38, and 39.

The initial distributions for ln C and m used in this study are considered multivariate Gaussian.[23] All the initial samples of the parameter b are set as zero because the initial bias is close to zero. The initial crack length is set as a range including the initial measured length. Similar to Ref. 2, the initial samples for the other parameters are created within a uniform range.

At each time step, N_p process noise samples will be sampled from a predefined distribution and assigned to the N_p particles. The noise distributions are determined through sources such as literature, as seen in this study, where authors Li et al.[2,5,6] have been consulted, or alternatively, through a trial-and-error approach.

Table 4. Particle filter parameters.

PF parameters used for all three models		
Number of particles N_p	h in kernel smoothing	Standard deviation in the likelihood function
4000	0.1	0.02
Initial range for x (mm)	Initial value for b (−)	Distributions of process noise ω_b for b
$x_0 \sim \mathrm{U}(2.5,\ 3.5)$	$b_0 = 0$	$\omega_b \sim \mathcal{N}(0, 0.005^2)$
PF parameters used for Model 1 only		
Initial distributions for $\ln\ C\ \left[\ln \frac{\mathrm{mm}}{\mathrm{cycle}(\mathrm{MPa}\sqrt{mm})^{-m}}\right]$, m (–)	Distributions of process noises $\{\omega_1,\ \omega_c,\ \omega_m\}$ for x, $\ln\ C$, m	
$\begin{bmatrix} \ln\ C_0 \\ m_0 \end{bmatrix} \sim \mathcal{N}\left(\begin{bmatrix} -45.01 \\ 6.117 \end{bmatrix}, \begin{bmatrix} 0.9966 & -0.1764 \\ -0.1764 & 0.0346 \end{bmatrix}\right)$	$\omega_1 \sim \mathcal{N}\left(-\frac{0.01^2}{2}, 0.01^2\right)$	$\omega_c \sim \mathcal{N}(0, 0.01^2)$ $\omega_m \sim \mathcal{N}(0, 0.001^2)$
PF parameters used for Model 2 only		
Initial range for $\{p_{l,0} : l = 1, 2, 3, 4\}$	Distributions of process noises $\{\omega_{p,l} : l = 1, 2, 3, 4\}$ for $\{p_l : l = 1, 2, 3, 4\}$	Distribution of process noise ω_1 for x
$p_{l,0} \sim \mathrm{U}(0.8p_{f,l}, 1.2p_{f,l})$	$\omega_{p,l} \sim \mathcal{N}\left(0, (0.00015p_{f,l})^2\right)$	$\omega_1 \sim \mathcal{N}\left(-\frac{0.01^2}{2}, 0.01^2\right)$
PF parameters used for Model 3 only		
Initial range for $\{q_{l,0} : l = 1, 2, 3, 4\}$	Distributions of process noises $\{\omega_{q,l} : l = 1, 2, 3, 4\}$ for $\{q_l : l = 1, 2, 3, 4\}$	Distributions of process noise ω_2 for x
$q_{l,0} \sim \mathrm{U}(0.8q_{f,l}, 1.2q_{f,l})$	$\omega_{q,l} \sim \mathcal{N}\left(0, (0.00015q_{f,l})^2\right)$	$\omega_2 \sim \mathcal{N}(0, 0.01^2)$

(i) The means of the distribution of $\begin{bmatrix} \ln\ C_0 \\ m_0 \end{bmatrix}$ are fitted from the crack growth data of specimen S6, and they are −45.01, and 6.117, respectively and (ii) $p_{f,l}$ and $q_{f,l}$ are the l-th coefficient of the third polynomial fitting function of Models (2) and (3), respectively, and they are fitted from the crack growth data of specimen S6.
PF: particle filter.

By considering a zero-mean Gaussian distribution for the measurement noise, the likelihood function is structured as:

$$p\left(y_k | \boldsymbol{z}_{l,k}^i\right) = \frac{1}{\sqrt{2\pi}\sigma_y} \exp\left(-\frac{1}{2\sigma_y{}^2}\left(y_k - y_k^i\right)^2\right) \quad (16)$$

where y_k^i is the observation calculated by the particle $\boldsymbol{z}_{l,k}^i$, and σ_y can be set as the STD of the measurement noise. In different applications, σ_y can be either empirically selected[24,40] or calculated from the data.[29,41]

Target crack growth and features

The crack lengths and the Lamb waves in this experiment are collected every several thousand load cycles. For simulating a more realistic SHM case, where the Lamb waves can be collected over shorter load cycle intervals for crack length quantification, the crack growth and the features from each of the five experimental specimens (S1–S5) are used to create the target crack lengths and the corresponding features at a shorter cycle interval through the procedure below.[5]

(i) The target crack lengths for each specimen are created every 300 load cycles through linear interpolation by the crack data provided in the section "Experimental study," and then corrupted by white Gaussian noise with a signal-to-noise ratio (SNR) of 50 dB to introduce some uncertainties in the crack growth process, as shown in Figure 7(a).
(ii) For each specimen, linear interpolation is applied to create the RMS-based feature at each target length, which is then corrupted by white Gaussian noise with an SNR of 30 dB to simulate the measurement noise, as given in Figure 7(b).

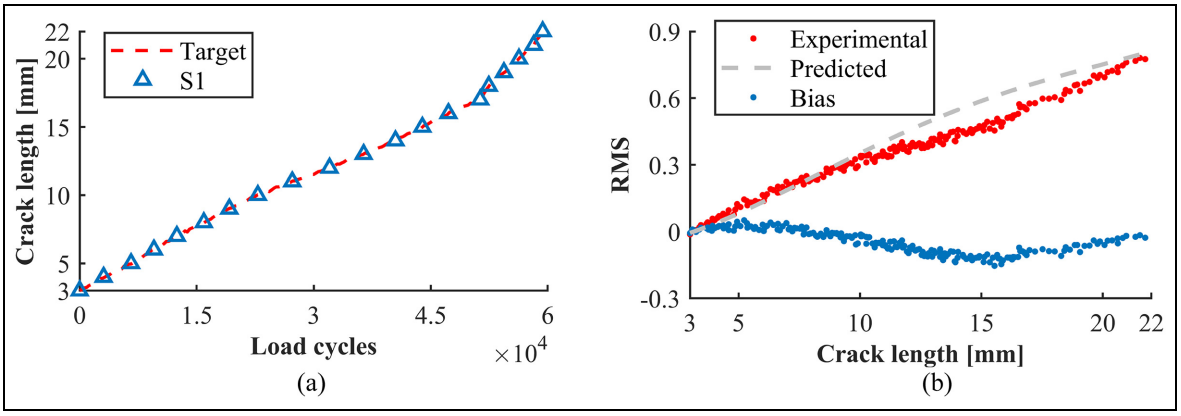

Figure 7. Target crack growth, RMS features, and bias: (a) target crack growth and (b) RMS features and bias.
RMS: root mean square.

Application results

This section provides a comprehensive comparison between the performances of traditional methods resorting to each degradation model and between those of traditional and new methods. The section "Traditional method for specimen S1" presents the estimation and prognostic results of specimen S1 from the traditional method resorting to each of the three degradation models, while section "New method for specimen S2" illustrates those from the new method by fusing all three models. The robustness of the proposed method among all the other specimens is validated in the section "Results from all the other specimens."

Traditional method for specimen S1

The traditional method applies one PF to one prognostic model to provide one group of estimates of the crack length and degradation parameters, which are then adopted for projecting the future state and RUL. Then, the samples of crack length and RUL from all three PFs are simply merged at each time step (called "simple fusion") for comparison. Those results are plotted in Appendix A1. Provided with satisfactory bias estimation, the samples of crack length from each model or simple fusion have the average values remaining close to the target values and their confidence boundaries (CBs) shrinking with the load cycle step, and the samples of those degradation parameters reduce their spread over load cycle steps, indicating a successful convergence.

The future crack lengths predicted based on the PF estimates at 3.6×10^4 load cycles are given in Figure A4, where the blue dashed line, the gray dotted line, and the gray histogram denote the estimated crack length, the crack length prediction trajectory, and the RUL posterior PDF, respectively. In general, each group of future states is distributed around the true crack lengths. This is also observed in Figure A5, where the average RUL is close to the target RUL, and the CBs shrink with the increasing load cycle steps. The above observations are the same as those in Refs. 5 and 6, where the traditional method resorting to one prognostic model has been applied to the same experimental study.

On the other hand, the estimation and prognostic performances using each model are different, which are then quantified by three metrics, that is, the root mean square error (RMSE) for the crack length estimation, the cumulative relative accuracy (CRA) for the RUL prediction, and the prognostic horizon (PH) for the RUL prediction, respectively. They are described as follows:

$$\mathrm{RMSE}=\sqrt{\frac{1}{T}\sum_{k=1}^{T}\left(\bar{x}_k-x_{\mathrm{true},k}\right)^2} \tag{17}$$

$$\mathrm{CRA}=\frac{1}{T-1}\sum_{k=1}^{T-1}\left(1-\frac{\left|\overline{\mathrm{RUL}}_k-\mathrm{RUL}_{\mathrm{true},k}\right|}{\mathrm{RUL}_{\mathrm{true},k}}\right) \tag{18}$$

where $\bar{x}$ and $\overline{\mathrm{RUL}}$ denote the mean of posterior estimates of the crack length and that of the RUL, respectively, the subscript "true" means the true crack length or RUL, and T is the number of discrete load cycle steps required by the PF until failure is reached.

PH is usually taken as the difference between the load cycle step of the latest measurement and the failure threshold, provided the RUL prediction at that step meets a pre-defined specification.[42] Following the strategy proposed in Corbetta et al.,[23] this study considers the PH as the number of load cycles when 60%

Table 5. Estimation and prognostic performances from traditional method resorting to one degradation model for specimen S1.

	Traditional method using one degradation model			Simple fusion
Which model	1	2	3	–
RMSE (mm)	1.175	1.640	**0.796**	0.961
CRA	0.536	0.584	**0.807**	0.753
PH (load cycles)	5400	30600	**33600**	5700

The smallest RMSE, largest PH, or highest CRA means the "best" performance, and those from the results of the traditional method are highlighted in bold.
RMSE: root mean square error; CRA: cumulative relative accuracy; PH: prognostic horizon.

Table 6. Estimation and prognostic performances by adopting one degradation model (traditional method) and by fusing multiple models (new method) for specimen S1.

	Traditional method using one degradation model			Simple fusion	Proposed method	
					Fusion 1 (crossover)	Fusion 2 (mutation)
Which model	1	2	3	–	–	–
RMSE (mm)	1.175	1.640	**0.796**	0.961	***0.338***	***0.402***
CRA	0.536	0.584	**0.807**	0.753	***0.870***	***0.884***
PH (load cycles)	5400	30,600	**33,600**	5700	***27,300***	***27,600***

(i) The smallest RMSE, largest PH, or highest CRA means the "best" performance, and those from the results of the traditional method are highlighted in bold and (ii) the result from the new method is highlighted in bold italic if it is more accurate than that from simple fusion. Same below.
RMSE: root mean square error; CRA: cumulative relative accuracy; PH: prognostic horizon.

of the RUL distribution first falls within a range of "true RUL$\pm$10%N." Lower RMSE, higher CRA, and larger PH represent better estimation and prognosis performances, respectively.

Table 5 presents the RMSEs, CRAs, and PHs for specimen S1, where, despite that the parameters of each degradation model are online estimated for compensating the uncertainties, the three models still yield different performances for the same specimen. The performance of simple fusion does not show a significant improvement because it is just a simple mixture of the three groups of estimates.

New method for specimen S1

The proposed method has each of the three prognostic models processed through one PF at each step, then applies all the estimates for crack length quantification and RUL prediction, and finally modifies the distribution of samples of the two shared components (i.e., crack length and bias) for each PF through either the crossover or mutation operator. Note that the two operators are separately inserted into the proposed method, providing two sets of results of crack length quantification and RUL prediction, and they are defined as "Fusion 1" and "Fusion 2," respectively.

Figures 8 and 9 show the crack length and bias estimation and the parameter estimation, respectively. The future state and RUL prediction are given in Figure 10. The general conclusions relating to those performances are similar to those arising from Appendix A1, thus not repeated here. On the other hand, the CB width of crack length or bias from the new method is narrower than that from the traditional method resorting to any of the three models. This is because the proposed method has the samples from each model interacting with those from the other two models, bringing a narrower posterior PDF that can fit with the three models. One may argue that this method has improved the particle diversity and should produce larger CBs. Indeed, larger diversity means that there are fewer same particles for each PF, which is not directly associated with the width of CB. The same phenomenon can be observed in future state and RUL prediction, where the RUL posterior PDF or CB width from the new method is narrower than that produced by the traditional method.

Table 6 presents the comparison between the performances of the traditional and the new methods, where the new method using either the crossover or mutation operator always performs more accurate crack length quantification and RUL prediction over the simple

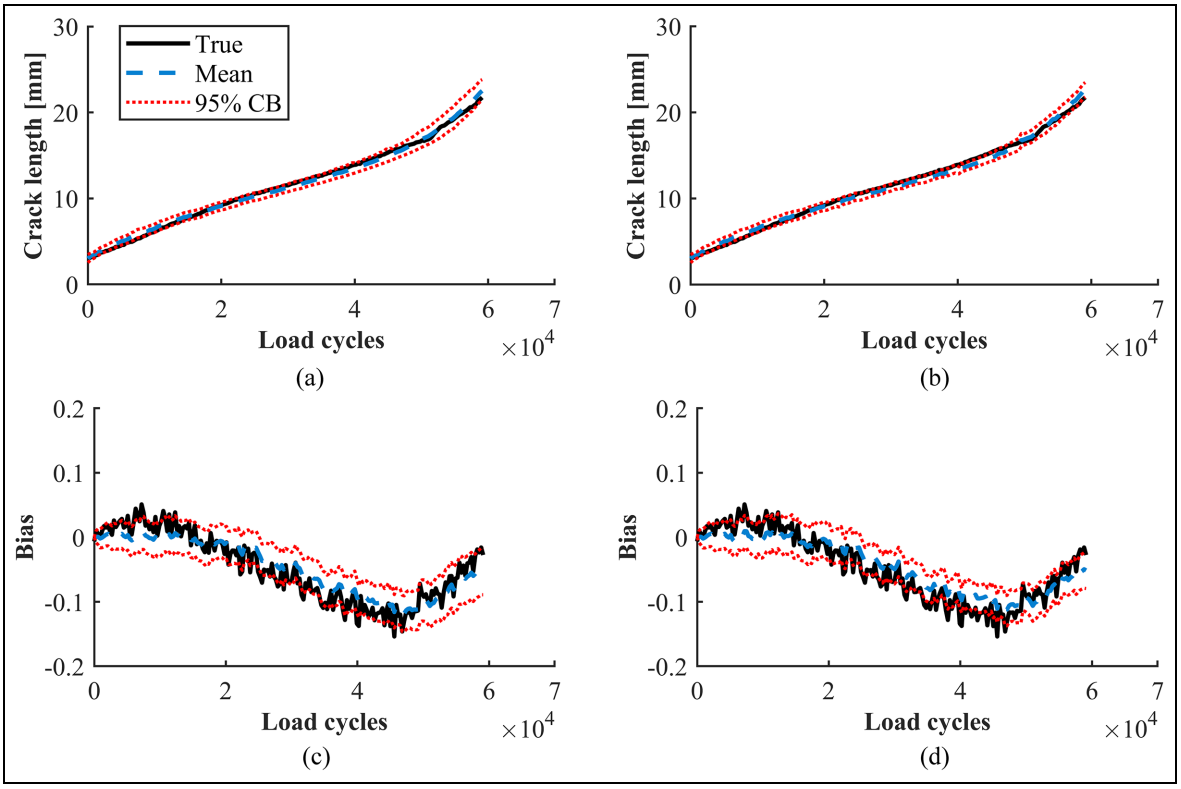

Figure 8. Estimation results of crack length and bias using new method for specimen S1: (a) Fusion 1, length estimation, (b) Fusion 2, length estimation, (c) Fusion 1, bias estimation, and (d) Fusion 2, bias estimation.
CB: confidence boundary.

fusion, which confirms that the fusion scheme for improving the particle diversity can yield better prognostic performance. Although the proposed method does not exhibit a significant improvement compared to the use of the traditional method with the third degradation model (which is the most effective among the three models), this does not reduce the significance of the proposed approach. This is because the prognostic model that delivers the best performance can vary among different specimens, and it is exceedingly challenging to predict, as detailed in the section "Results from all the other specimens."

Results from all the other specimens

The robustness of the proposed framework is now tested with the specimens S2–S5. The analyses in sections "Traditional method for specimen S1" and "New method for specimen S2" are repeated with the same PF parameters given in the section "State space modeling and PF parameters." The crack length estimation and RUL prediction results using the new method are presented in Figures 11 and 12, respectively, which lead to the same conclusions drawn from Figures 8 and 10, and then demonstrate the robustness of the proposed method over different specimens.

Tables 7–10 show the estimation and prognostic performances from specimens S2–S5, respectively. When resorting to the traditional method, the model providing the best prognostic performance can be different among different specimens, or even, by using different performance metrics. For example, when the traditional method is applied to specimen S4, the results from Model (1) have the smallest RMSE and the largest CRA, while the results from Model (3) have the largest PH.

In general, the proposed method yields better performance than the use of simple fusion, demonstrating the robustness of this method, but it does not always guarantee superior performance over the traditional method resorting to the best model for each specimen. The latter, however, never degrades the value of this method, as already discussed above.

Conclusions

Damage prognosis methods typically require a properly selected degradation model describing the damage

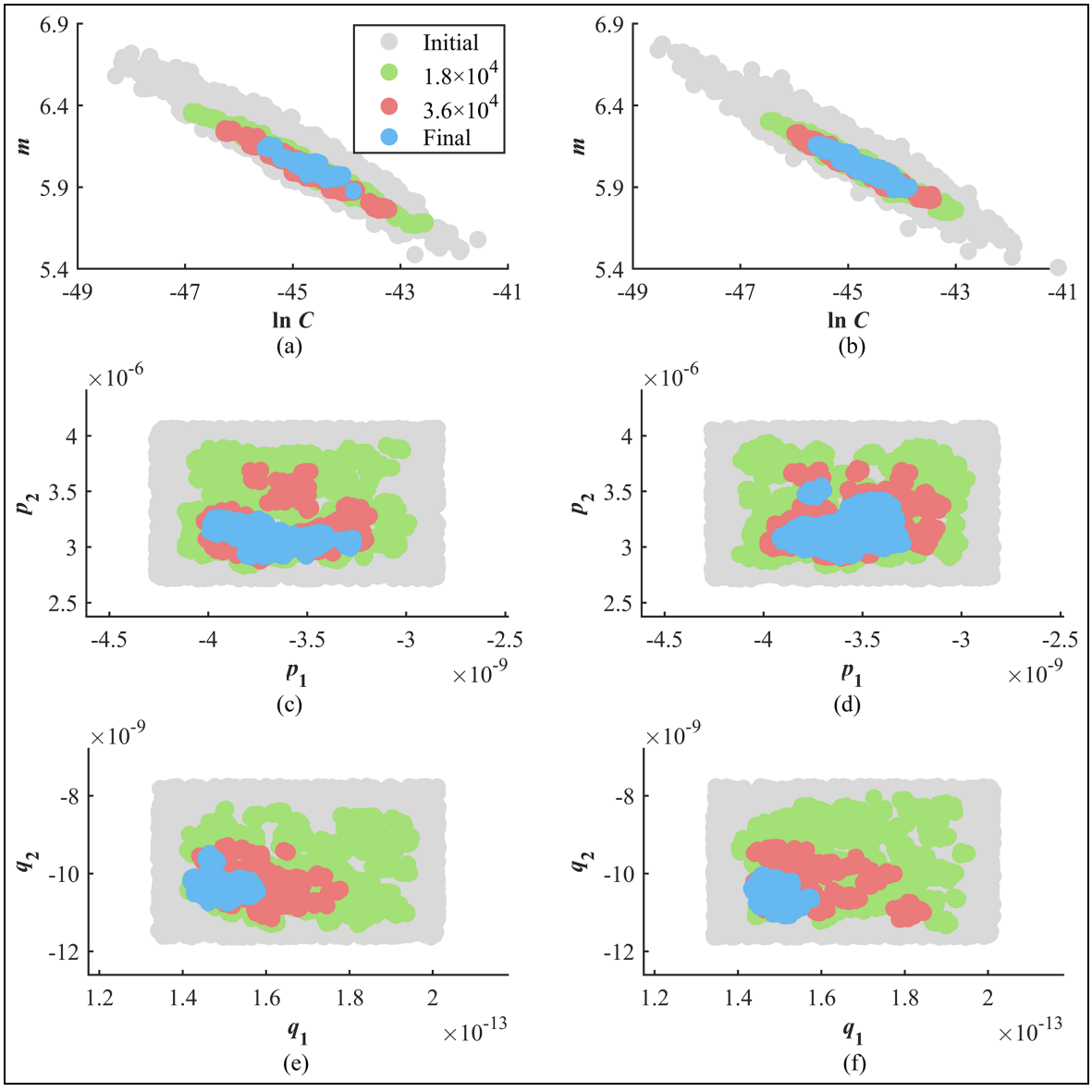

Figure 9. Estimation results of model parameters using a new method for specimen S1: (a) Fusion 1, parameters ln C and m, (b) Fusion 2, parameters ln C and m, (c) Fusion 1, parameters p_1 and p_2, (d) Fusion 2, parameters p_1 and p_2, (e) Fusion 1, parameters q_1 and q_2, and (f) Fusion 2, parameters q_1 and q_2.
Note that "Initial," "1.8×10^4," "3.6×10^4," and "Final" within the legend represent the samples of the three parameters at 0, 1.8×10^4, 3.6×10^4, and last load cycles, respectively.

growth with time or load cycle steps. To provide a more robust prognostic performance, this work has proposed a PF-based damage prognosis framework by fusing multiple degradation models.

The results of the traditional and new methods can lead to the following conclusions. When using the traditional method of relying on one degradation model, it is important to note that the best degradation model can differ among the five specimens and also vary depending on the performance metrics used. Simply combining the estimates from multiple models does not enhance the accuracies of crack length quantification and RUL prediction. In all of the five specimens evaluated, the new method, leveraging either the crossover or mutation operator, consistently outperforms the simple mixture mentioned above, attesting to its robustness.

Based on the results presented in this paper, it can be concluded that the proposed method offers a promising alternative to the traditional approach. While the proposed method may not always result in superior performance compared to the best model-based

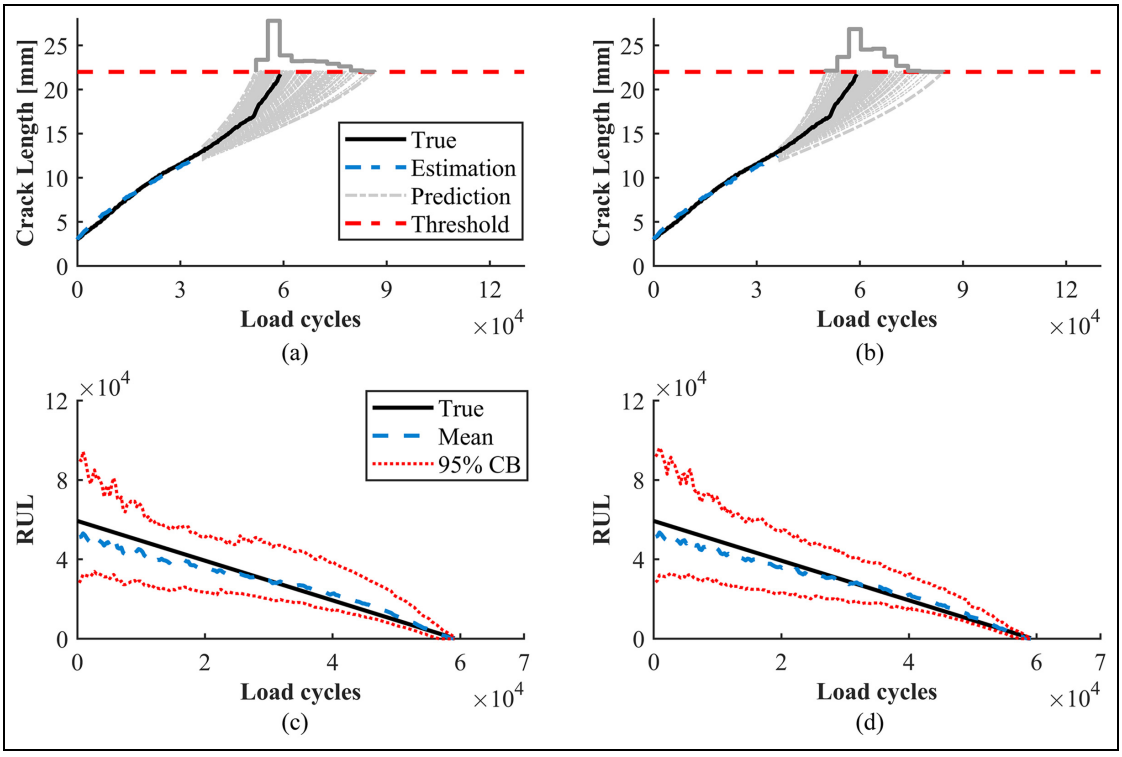

Figure 10. Future state prediction at 3.6×10^4 load cycles and RUL prediction using a new method for specimen S1: (a) Fusion 1, future state prediction, (b) Fusion 2, future state prediction, (c) Fusion 1, RUL prediction, and (d) Fusion 2, RUL prediction.
RUL: remaining useful life.

Table 7. Estimation and prognostic performances by adopting one degradation model (traditional method) and by fusing multiple models (new method) for specimen S2.

	Traditional method using one degradation model			Simple fusion	Proposed method	
					Fusion 1 (crossover)	Fusion 2 (mutation)
Which model	1	2	3	–	–	–
RMSE (mm)	**1.250**	1.381	2.050	1.109	***0.829***	1.290
CRA	0.382	**0.801**	0.588	0.784	***0.831***	***0.814***
PH (load cycles)	4800	**43,200**	6600	6600	***20,100***	***14,400***

(i) The smallest RMSE, largest PH, or highest CRA means the "best" performance, and those from the results of the traditional method are highlighted in bold and (ii) the result from the new method is highlighted in bold italic if it is more accurate than that from simple fusion.
RMSE: root mean square error; CRA: cumulative relative accuracy; PH: prognostic horizon.

Table 8. Estimation and prognostic performances by adopting one degradation model (traditional method) and by fusing multiple models (new method) for specimen S3.

	Traditional method using one degradation model			Simple fusion	Proposed method	
					Fusion 1 (crossover)	Fusion 2 (mutation)
Which model	1	2	3	–	–	–
RMSE (mm)	1.206	1.694	**0.996**	0.884	***0.716***	***0.256***
CRA	0.423	0.175	**0.561**	0.429	***0.470***	***0.730***
PH (load cycles)	**40,500**	3600	39,000	4200	***28,200***	***26,400***

(i) The smallest RMSE, largest PH, or highest CRA means the "best" performance, and those from the results of the traditional method are highlighted in bold and (ii) the result from the new method is highlighted in bold italic if it is more accurate than that from simple fusion.
RMSE: root mean square error; CRA: cumulative relative accuracy; PH: prognostic horizon.

Table 9. Estimation and prognostic performances by adopting one degradation model (traditional method) and by fusing multiple models (new method) for specimen S4.

	Traditional method using one degradation model			Simple fusion	Proposed method	
					Fusion 1 (crossover)	Fusion 2 (mutation)
Which model	1	2	3	–	–	–
RMSE (mm)	**0.685**	1.584	1.072	1.006	***0.665***	***0.670***
CRA	**0.592**	0.582	0.477	0.580	***0.688***	***0.670***
PH (load cycles)	29400	4200	**38400**	4200	***25800***	***7200***

(i) The smallest RMSE, largest PH, or highest CRA means the "best" performance, and those from the results of the traditional method are highlighted in bold and (ii) the result from the new method is highlighted in bold italic if it is more accurate than that from simple fusion.
RMSE: root mean square error; CRA: cumulative relative accuracy; PH: prognostic horizon.

Table 10. Estimation and prognostic performances by adopting one degradation model (traditional method) and by fusing multiple models (new method) for specimen S5.

	Traditional method using one degradation model			Simple fusion	Proposed method	
					Fusion 1 (crossover)	Fusion 2 (mutation)
Which model	1	2	3	–	–	–
RMSE (mm)	1.059	**0.951**	1.533	0.962	***0.446***	***0.713***
CRA	0.548	**0.762**	0.659	0.830	***0.868***	***0.834***
PH (load cycles)	4500	**36,900**	28,800	24,600	***28,500***	***29,400***

(i) The smallest RMSE, largest PH, or highest CRA means the "best" performance, and those from the results of the traditional method are highlighted in bold and (ii) the result from the new method is highlighted in bold italic if it is more accurate than that from simple fusion.
RMSE: root mean square error; CRA: cumulative relative accuracy; PH: prognostic horizon.

traditional approach, it addresses the uncertainty involved in determining the most effective model in advance. Furthermore, the proposed method provides a more comprehensive evaluation of the degradation behavior by considering multiple models, which can enhance the accuracy of damage quantification and RUL prediction.

In a more practical application scenario where tens of or hundreds of available degradation models are available, some of those models may consistently provide inaccurate crack length quantification and RUL prediction results, thereby compromising the performance of the proposed method if such models are included. Consequently, it is necessary to develop an offline or online scheme to select a list of "good" degradation models or "good" samples. Moreover, the proposed method requires all the prognostic models to share specific state components like crack length, which may not always be possible, especially considering that some data-driven models only include some sort of data-driven HI. A necessary extension has to be made in the case of no shared state component. Finally, it should be noted that the proposed approach requires the use of multiple PFs; thus, its computation time will linearly increase with the number of models (or PFs) used. However, this issue can be addressed by developing computationally efficient PFs, which will enable the use of more models without significantly increasing computation time and enhance the practical applicability of the proposed method.

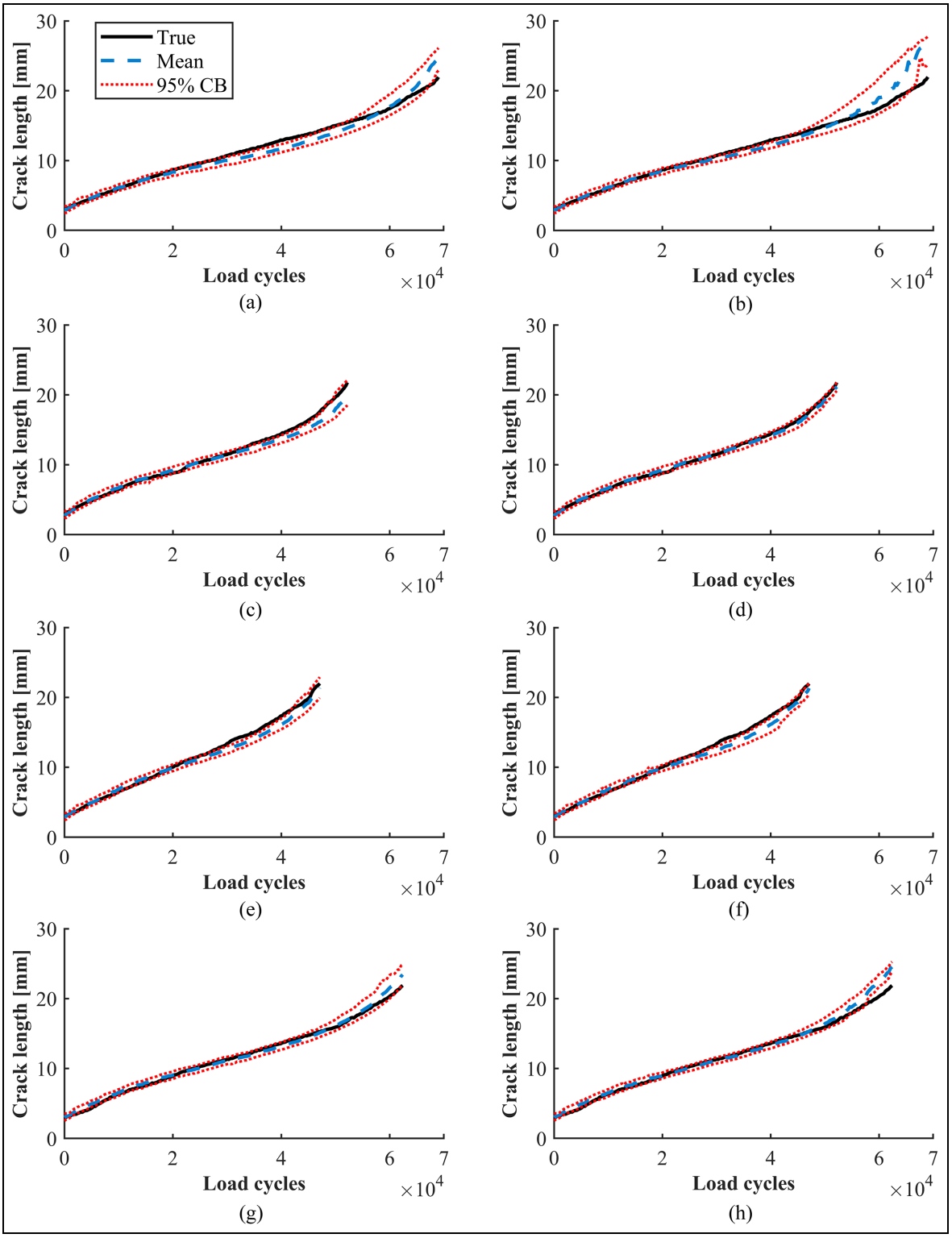

Figure 11 Crack length estimations from a new method for specimens S2–S5: (a) Fusion 1, S2, (b) Fusion 2, S2, (c) Fusion 1, S3, (d) Fusion 2, S3, (e) Fusion 1, S4, (f) Fusion 2, S4, (g) Fusion 1, S5, and (h) Fusion 2, S5.
CB: confidence boundary; RUL: remaining useful life.

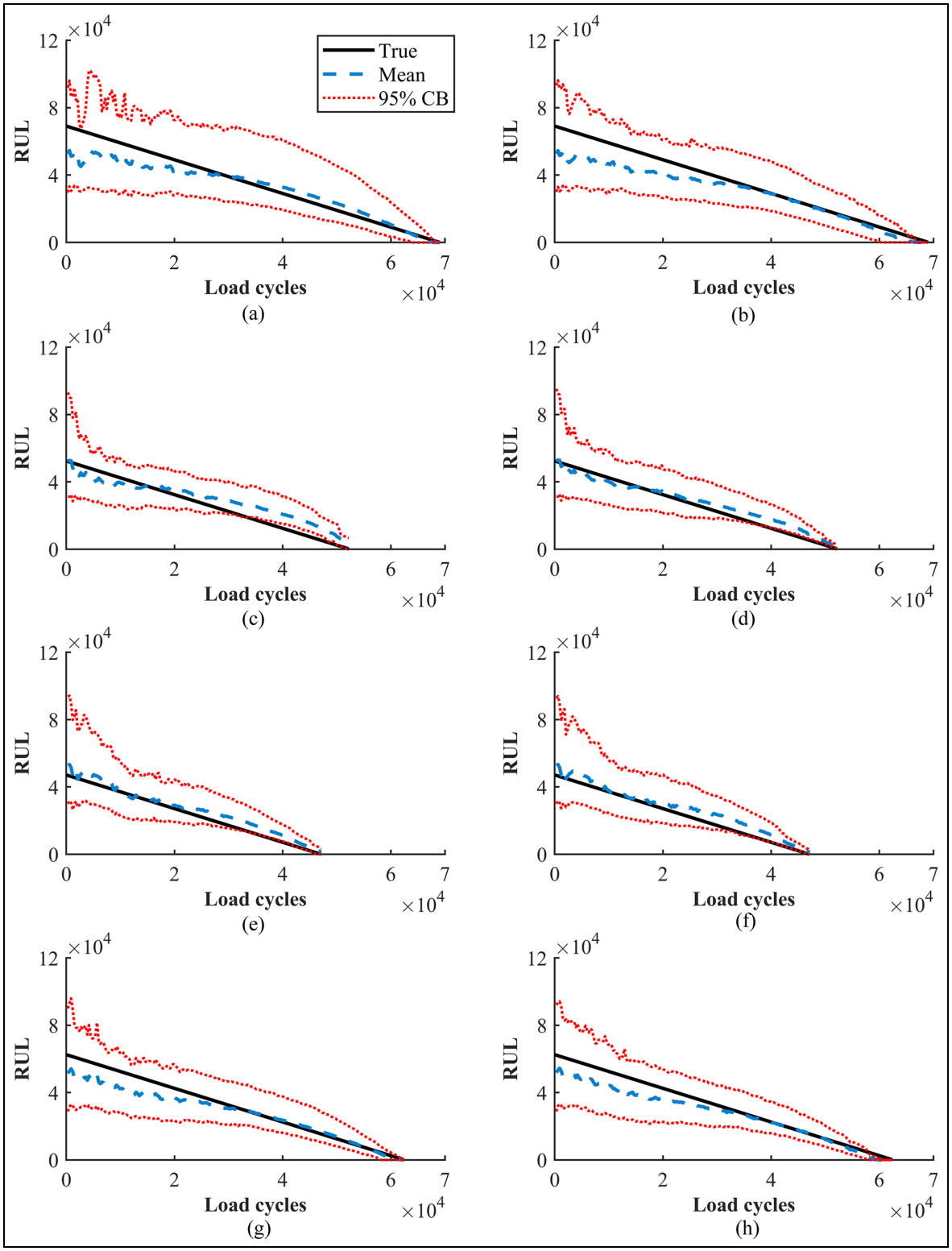

Figure 12. RUL predictions from a new method for specimens S2–S5: (a) Fusion 1, S2, (b) Fusion 2, S2, (c) Fusion 1, S3, (d) Fusion 2, S3, (e) Fusion 1, S4, (f) Fusion 2, S4, (g) Fusion 1, S5, and (h) Fusion 2, S5.
CB: confidence boundary; RUL: remaining useful life.

Declaration of conflicting interests

The author(s) declared no potential conflicts of interest with respect to the research, authorship, and/or publication of this article.

Funding

The author(s) disclosed receipt of the following financial support for the research, authorship, and/or publication of this article: This project has received funding from the European Union's Horizon 2020 research and innovation program under the Marie Skłodowska-Curie grant agreement No. 859957.

ORCID iDs

Tianzhi Li https://orcid.org/0000-0001-6196-9948
Jian Chen https://orcid.org/0000-0002-5991-0805
Shenfang Yuan https://orcid.org/0000-0003-0154-1231

References

1. Chiachío M, Chiachío J, Sankararaman S, et al. A new algorithm for prognostics using subset simulation. *Reliab Eng Syst Saf* 2017; 168: 189–199.
2. Li T, Cadini F, Chiachío M, et al. Particle filter-based delamination shape prediction in composites subjected to fatigue loading. *Struct Health Monit*. Epub ahead of print 8 August 2022. DOI: 10.1177/14759217221116041.
3. Tao C, Zhang C, Ji H, et al. Application of neural network to model stiffness degradation for composite laminates under cyclic loadings. *Compos Sci Technol* 2021; 203: 108573.
4. Yue N, Broer A, Briand W, et al. Assessing stiffness degradation of stiffened composite panels in post-buckling compression-compression fatigue using guided waves. *Compos Struct* 2022; 293: 115751.
5. Li T, Lomazzi L, Cadini F, et al. Numerical simulation-aided particle filter-based damage prognosis using Lamb waves. *Mech Syst Signal Process* 2022; 178: 109326.
6. Li T, Sbarufatti C, Cadini F, et al. Particle filter-based hybrid damage prognosis considering measurement bias. *Struct Control Health Monit* 2021; 29: e2914.
7. Cadini F, Sbarufatti C, Corbetta M, et al. Particle filtering-based adaptive training of neural networks for real-time structural damage diagnosis and prognosis. *Struct Control Health Monit* 2019; 26: e2451.
8. Cadini F, Sbarufatti C, Corbetta M, et al. A particle filter-based model selection algorithm for fatigue damage identification on aeronautical structures. *Struct Control Health Monit* 2017; 24: e2002.
9. Zhou X, He S, Dong L, et al. Real-time prediction of probabilistic crack growth with a helicopter component Digital Twin. *AIAA J* 2022; 60: 2555–2567.
10. Moradi M, Broer A, Chiachío J, et al. Intelligent health indicator construction for prognostics of composite structures utilizing a semi-supervised deep neural network and SHM data. *Eng Appl Artif Intell* 2023; 117: 105502.
11. Eleftheroglou N, Zarouchas D and Benedictus R. An adaptive probabilistic data-driven methodology for prognosis of the fatigue life of composite structures. *Compos Struct* 2020; 245: 112386.
12. Liu X, Lei Y, Li N, et al. RUL prediction of machinery using convolutional-vector fusion network through multi-feature dynamic weighting. *Mech Syst Signal Process* 2023; 185: 109788.
13. Galanopoulos G, Eleftheroglou N, Milanoski D, et al. A novel strain-based health indicator for the remaining useful life estimation of degrading composite structures. *Compos Struct* 2023; 306: 116579.
14. Zhao F, Zhou X, Wang C, et al. Setting adaptive inspection intervals in helicopter components, based on a Digital Twin. *AIAA J*. Epub ahead of print 18 February 2023. DOI: 10.2514/1.J062222.
15. Lei Y, Li N, Guo L, et al. Machinery health prognostics: a systematic review from data acquisition to RUL prediction. *Mech Syst Signal Process* 2018; 104: 799–834.
16. Baraldi P, Mangili F and Zio E. Investigation of uncertainty treatment capability of model-based and data-driven prognostic methods using simulated data. *Reliab Eng Syst Saf* 2013; 112: 94–108.
17. Lopez I and Sarigul-Klijn N. A review of uncertainty in flight vehicle structural damage monitoring, diagnosis and control: challenges and opportunities. *Prog Aerosp Sci* 2010; 46: 247–273.
18. Guha A and Patra A. State of health estimation of lithium-ion batteries using capacity fade and internal resistance growth models. *IEEE Trans Transp Electrif* 2018; 4: 135–146.
19. Xing Y, Ma EWM, Tsui K-L, et al. An ensemble model for predicting the remaining useful performance of lithium-ion batteries. *Microelectron Reliab* 2013; 53: 811–820.
20. Su X, Wang S, Pecht M, et al. Interacting multiple model particle filter for prognostics of lithium-ion batteries. *Microelectron Reliab* 2017; 70: 59–69.
21. Guan X, Jha R and Liu Y. Model selection, updating, and averaging for probabilistic fatigue damage prognosis. *Struct Safety* 2011; 33: 242–249.
22. Zhang D, Baraldi P, Cadet C, et al. An ensemble of models for integrating dependent sources of information for the prognosis of the remaining useful life of proton exchange membrane fuel cells. *Mech Syst Signal Process* 2019; 124: 479–501.
23. Corbetta M, Sbarufatti C, Giglio M, et al. Optimization of nonlinear, non-Gaussian Bayesian filtering for diagnosis and prognosis of monotonic degradation processes. *Mech Syst Signal Process* 2018; 104: 305–322.
24. Corbetta M, Sbarufatti C, Giglio M, et al. A Bayesian framework for fatigue life prediction of composite laminates under co-existing matrix cracks and delamination. *Compos Struct* 2018; 187: 58–70.
25. Chiachío J, Chiachío M, Sankararaman S, et al. Condition-based prediction of time-dependent reliability in composites. *Reliab Eng Syst Safety* 2015; 142: 134–147.
26. Cristiani D, Sbarufatti C and Giglio M. Damage diagnosis and prognosis in composite double cantilever beam

coupons by particle filtering and surrogate modelling. *Struct Health Monit* 2020; 20: 147592172096006.
27. Cristiani D, Sbarufatti C, Cadini F, et al. Fatigue damage diagnosis and prognosis of an aeronautical structure based on surrogate modelling and particle filter. *Struct Health Monit* 2021; 20: 2726–2746.
28. Chen J, Yuan S and Wang H. On-line updating Gaussian process measurement model for crack prognosis using the particle filter. *Mech Syst Signal Process* 2020; 140: 106646.
29. Chen J, Yuan S and Jin X. On-line prognosis of fatigue cracking via a regularized particle filter and guided wave monitoring. *Mech Syst Signal Process* 2019; 131: 1–17.
30. Arulampalam MS, Maskell S, Gordon N, et al. A tutorial on particle filters for online nonlinear/non-Gaussian Bayesian tracking. *IEEE Trans Signal Process* 2002; 50: 174–188.
31. Yin S and Zhu X. Intelligent particle filter and its application to fault detection of nonlinear system. *IEEE Trans Ind Electron* 2015; 62: 3852–3861.
32. Yin S, Zhu X, Qiu J, et al. State estimation in nonlinear system using sequential evolutionary filter. *IEEE Trans Ind Electron* 2016; 63: 3786–3794.
33. Wang X, Li T, Sun S, et al. A survey of recent advances in particle filters and remaining challenges for multitarget tracking. *Sensors* 2017; 17: 2707.
34. Li T, Sun S, Sattar TP, et al. Fight sample degeneracy and impoverishment in particle filters: a review of intelligent approaches. *Expert Syst Appl* 2014; 41: 3944–3954.
35. Qiu L, Yuan S, Shi X, et al. Design of piezoelectric transducer layer with electromagnetic shielding and high connection reliability. *Smart Mater Struct* 2012; 21: 075032.
36. Buchaiah S and Shakya P. Bearing fault diagnosis and prognosis using data fusion based feature extraction and feature selection. *Measurement* 2022; 188: 110506.
37. Liu J and West M. Combined parameter and state estimation in simulation-based filtering. In: Doucet A, Freitas N and Gordon N (Eds), *Sequential Monte Carlo methods in practice*. New York, NY: Springer, 2001, pp. 197–223.
38. Chatzi EN and Smyth AW. The unscented Kalman filter and particle filter methods for nonlinear structural system identification with non-collocated heterogeneous sensing. *Struct Control Health Monit* 2010; 16: 99–123.
39. Yoo SJ, Jung DH, Kim JH, et al. A comparative study of soft sensor design for lipid estimation of microalgal photobioreactor system with experimental validation. *Bioresour Technol* 2015; 179: 275–283.
40. Chen C, Zhang B, Vachtsevanos G, et al. Machine condition prediction based on adaptive neuro–fuzzy and high-order particle filtering. *IEEE Trans Ind Electron* 2011; 58: 4353–4364.
41. Sajeeb R, Manohar CS and Roy D. A conditionally linearized Monte Carlo filter in non-linear structural dynamics. *Int J Non-Linear Mech* 2009; 44: 776–790.
42. Saxena A, Celaya J, Balaban E, et al. Metrics for evaluating performance of prognostic techniques. In: *2008 International conference on prognostics and health management*, Denver, 2008, pp. 1–17.

Appendix A1

The estimation and prognostic results of the traditional method using each of the three damage degradation models for specimen S1 are shown in Figures A1–A5, which are the crack length estimation, the crack growth parameter estimation (ln C and m), the bias estimation, the future state prediction, and the RUL prediction, respectively.

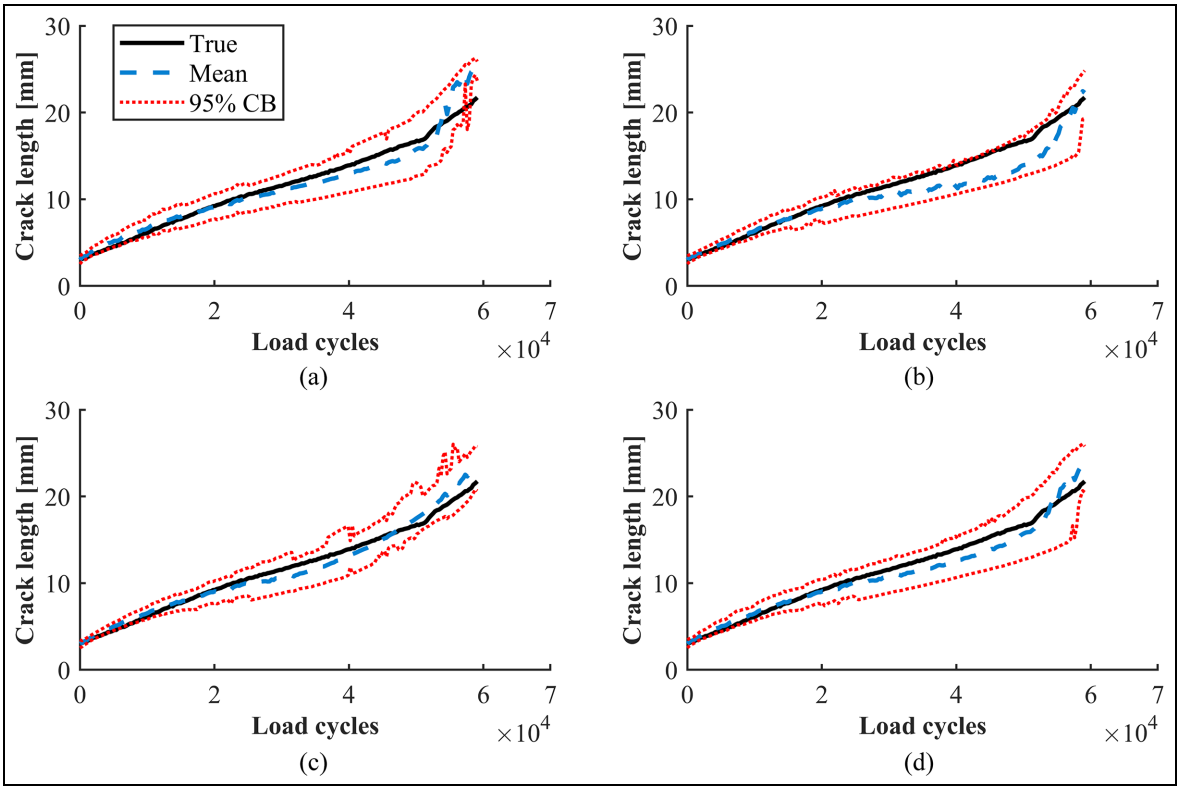

Figure A1 Crack length estimation using traditional method resorting to one degradation model for specimen S1: (a) Model 1, (b) Model 2, (c) Model 3, and (d) simple fusion.
CB: confidence boundary.

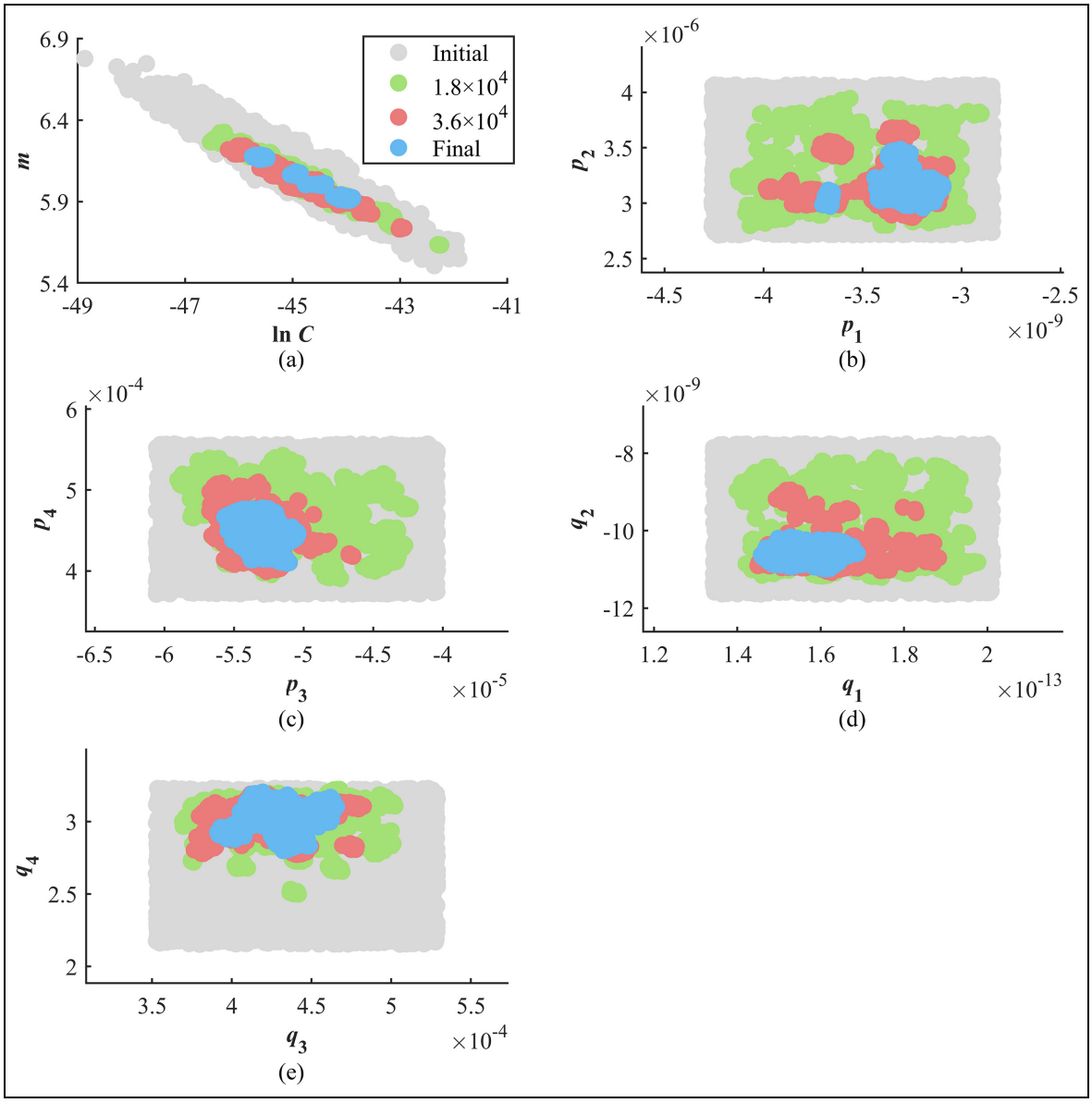

Figure A2. Parameter estimation using traditional method resorting to one degradation model for specimen S1: (a) Model 1, parameters ln C and m, (b) Model 2, parameters p_1 and p_2, (c) Model 2, parameters p_3 and p_4, (d) Model 3, parameters q_1 and q_2, and (e) Model 3, parameters q_3 and q_4.

Note that "Initial," "1.8×10^4," "3.6×10^4," and "Final" within the legend represent the samples of the three parameters at 0, 1.8×10^4, 3.6×10^4, and last load cycles, respectively.

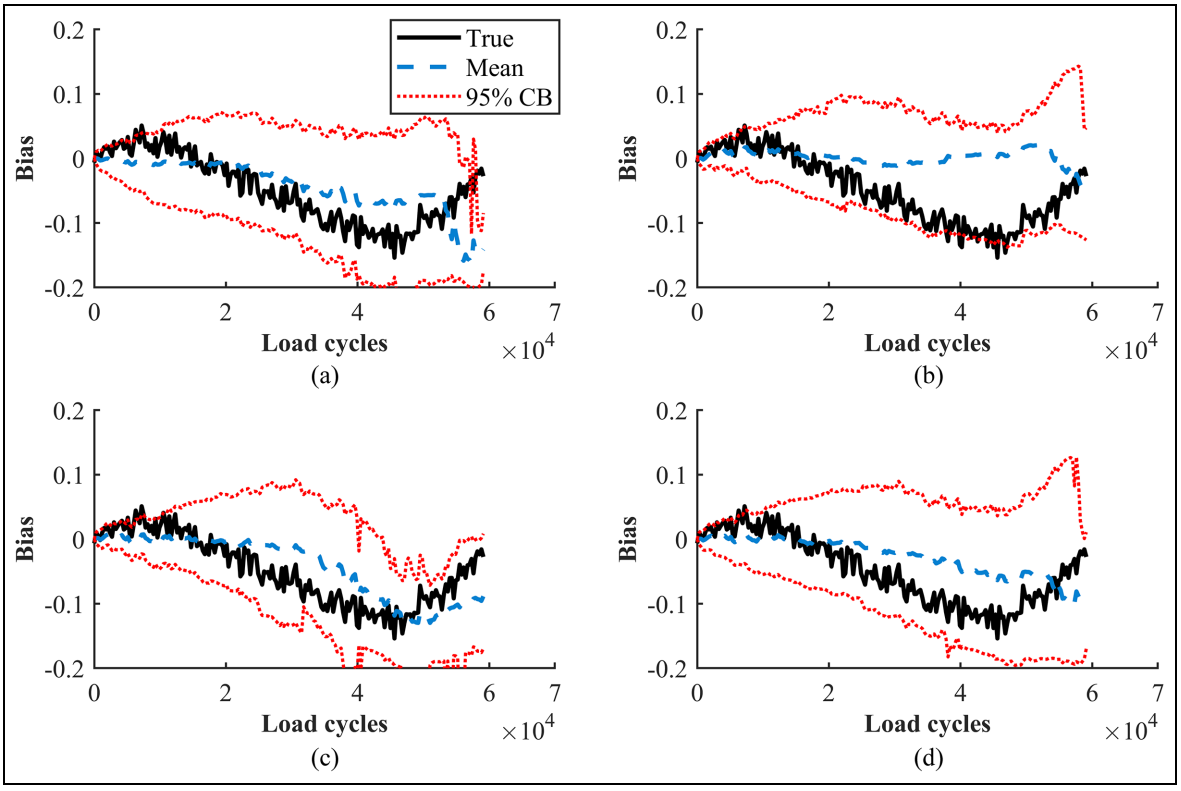

Figure A3. Bias estimation using traditional method resorting to one degradation model for specimen S1: (a) Model 1, (b) Model 2, (c) Model 3, and (d) simple fusion.

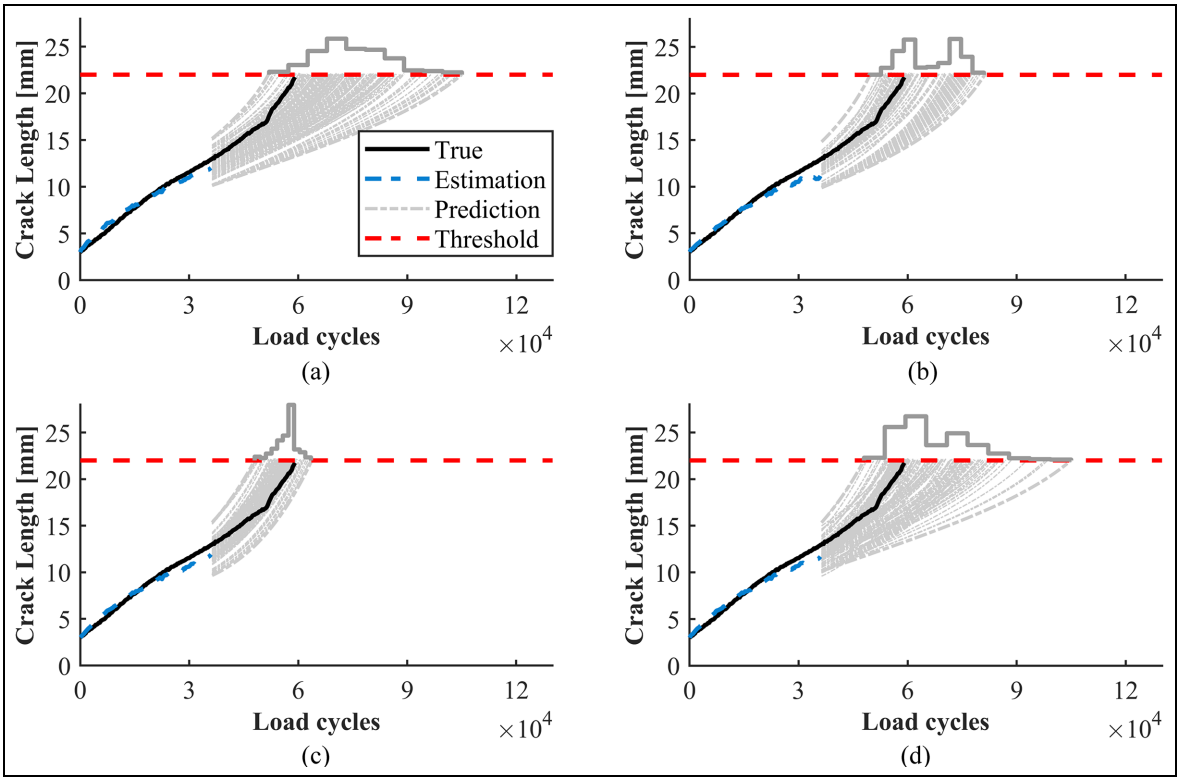

Figure A4. Future state prediction at 3.6×10^4 load cycles using traditional method resorting to one degradation model for specimen S1: (a) Model 1, (b) Model 2, (c) Model 3, and (d) simple fusion.

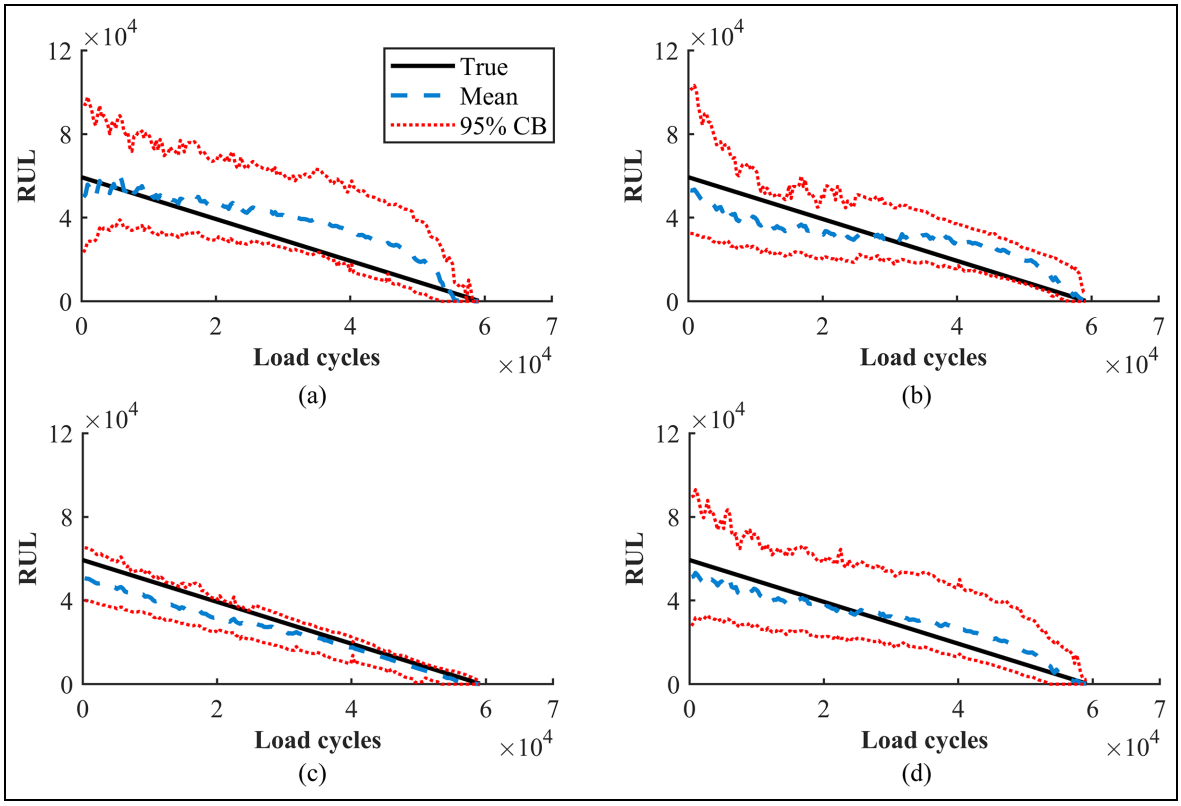

Figure A5. RUL prediction using traditional method resorting to one degradation model for specimen S1: (a) Model 1, (b) Model 2, (c) Model 3, and (d) simple fusion.
RUL: remaining useful life.